Available online at www.sciencedirect.com
ScienceDirect
Sensors and Actuators B 132 (2008) 531–539
SENSORS AND ACTUATORS B CHEMICAL
www.elsevier.com/locate/snb

Integrated and reusable in-plane microfluidic interconnects

Ronalee Lo, Ellis Meng *

Biomedical Microsystems Laboratory, Department of Biomedical Engineering, University of Southern California, 1042 Downy Way, DRB-140, Los Angeles, CA 90089-1111, United States

Available online 22 November 2007

Abstract

A concept for reusable, in-plane polymer microfluidic interconnects that are directly integrated into microfluidic systems is reported. Convenient, on-demand world-to-chip interfaces are established by utilizing a pin-and-socket approach in which commercially available non-coring syringe needles are manually inserted through predefined polydimethylsiloxane (PDMS) septa integrated at the inlets/outlets of microchannels. Receptacles for the septa were batch-fabricated in a single layer of SU-8 that also formed microchannels in the microfluidic system. Due to the self-sealing nature of PDMS, the septa were used repeatedly and withstood multiple needle insertions and removals without leakage. Needle pull-out force was modeled as debonding in a fiber/matrix system and evaluated experimentally both in single and multiple pull-out studies. Results were compared with other published interconnects of similar construction. Interconnects were also evaluated under pressurized conditions and tested to failure. The simple format of these interconnects is readily adapted to many microfluidic fabrication processes and thus can be easily incorporated into existing microfluidic systems.

Keywords: Microfluidics; Packaging; Interconnects; World-to-chip interface

1. Introduction

Microfluidics, and in particular micro total analysis systems (μTAS) and lab-on-a-chip (LOC), have many features advantageous for advanced chemical and biological analyses. The improved performance achieved in part through system miniaturization, laminar flow, high throughput, reduced sample consumption, and shorter analysis time has enabled new diagnostic tools and resulted in the application of these technologies to areas such as chemical synthesis, genetic analysis, drug screening, and even single cell/molecule analysis [1,2]. To realize the full potential of microfluidics, a suitable packaging technology to reliably couple micromachined channels to the macro-world is required.

The micro-to-macro fluidic interface, or interconnect, is usually a custom designed solution and assembled one at a time. This assembly process is time consuming and can require precision alignment or complicated fabrication steps. The lack of a batch-fabricated approach to interconnects greatly complicates the packaging of the microfluidic system and is an obstacle to the widespread commercialization of these microfluidic systems. Also, many interconnects have out-of-plane interfaces [3–11] in which the tubing and interconnect are connected perpendicularly with respect to the substrate surface. Out-of-plane interconnects can obstruct optical viewing of the microfluidic system and interfere with operation of microscope objectives. To accommodate microscope operation, interconnects are placed further apart which increases dead volume and overall system size. Robust mechanical connections in an out-of-plane approach are difficult to achieve due to limited contact area between the device and tubing. Adhesives can reinforce the connection [3,9,11], but are difficult to control; device yield is reduced when adhesive bleeds beyond the application area and clogs the microfluidic system. When a removable connection or modular approach is desired as opposed to a permanent connection, adhesives cannot be used. Most existing interconnects cannot be removed from the system without leaving a permanent fluidic breach in the system [3,4,6,8,9,11–13]. Thus, an alternative approach is required.

A novel interconnect is investigated to address the current challenges in microfluidics packaging. The interconnect design follows the plug-in format (pin-and-socket) found in microelectronics. In this case, the "pin" is a commercially-available, small diameter needle while the "socket" corresponds to an integrated polydimethylsiloxane (PDMS) septum contained within a SU-8 housing located at the inlet and/or outlet of a microfluidic system (Fig. 1). The SU-8 housing also serves as a needle insertion

* Corresponding author. Tel.: +1 213 740 6952; fax: +1 213 821 3897.
E-mail address: ellis.meng@usc.edu (E. Meng).

0925-4005/$ – see front matter © 2007 Elsevier B.V. All rights reserved.
doi:10.1016/j.snb.2007.11.024

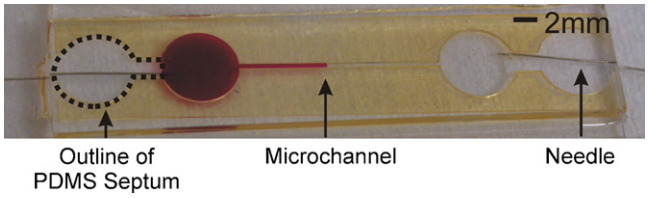

Fig. 1. Microfluidic system with integrated circular interconnects. 33-gauge non-coring needles were inserted into the input and output septums. Rhodamine was introduced into the system to demonstrate system functionality. PDMS septum is outlined to indicate its location.

guide and forms the microchannel between the inlet and outlet. The microfluidic system can be accessed by piercing a needle through the septum. By using a non-coring syringe needle, fluidic connections may be repeatedly established via septa; once the needle is removed, the PDMS septum reseals preserving the integrity of the microfluidic system and any contained fluids [14].

The in-plane layout of the interconnect, in which the interconnect is oriented in the same plane as the substrate, enables robust microfluidic connections by increasing the contact area between the macro-world needle and the microchannels in the chip. Connections are established on-demand and without the need for adhesives, precision alignment, thru-wafer drilling/etching, or other complex post-processing and assembly steps. Furthermore, the interconnect does not impede microscope observation of the system. This microfluidic interconnect approach incorporates packaging in the design and layout of the microfluidic system and can be batch-fabricated. These interconnects are easily adapted to other microfluidic system designs by simply adding a single mask to an existing fabrication process to create SU-8 anchors for the septums.

2. Theory

A needle inserted through a PDMS septum can be modeled as a stiff fiber embedded in a soft matrix. Total pull-out force, the force required to completely remove the needle from the PDMS septum, can be used as a measure of the strength of the interface between the needle and the septum. Debonding in this model system can be achieved by the application of tensile force, torque, or a compressive force, however, only the tension-induced debonding is considered here. Pull-out forces for fiber/matrix joints subjected to tension have been explained by Gent and Liu using a modified theory based on the Griffith fracture energy criterion for debonding that also accounts for the work associated with frictional sliding at the debonded interface [15]. The strength of adhesion is associated with the energy criterion for fracture and can be expressed as:

$$F_0^2 = 4\pi A r E_m G_a \tag{1}$$

where F_0 is the adhesion force, A is the cross-sectional area of the matrix, r is the fiber radius, E_m is the Young's modulus of the matrix material, and G_a is the adhesive fracture energy. The frictional pull-out force, F_f, is expressed as:

$$F_f = 2\pi r \mu p X \tag{2}$$

where r is the radius of the fiber; μ is the coefficient of friction; p is the compressive stress; and X is the contact length between the fiber and the matrix. This result assumes that the coefficient of friction is constant. If there is a 2% or greater pressure at the fiber tip compared to the Young's modulus of the matrix, then the product of the coefficient of friction and compressive stress can be represented by a constant value, $k = \mu p$. Under this condition, the coefficient of friction is independent of pressure and the overall force expression becomes:

$$F_f = 2\pi r k X \tag{3}$$

The total pull-out force, F, is a combination of the frictional and adhesion forces:

$$F = F_f + F_0 = 2\pi r k X + F_0 \tag{4}$$

and yields a linear relationship between the pull-out force and the fiber/matrix contact length. The strength of adhesion G_a is found from Eq. (1) by extrapolating the pull-out force F to the case where $X = 0$ to obtain the intercept F_0.

3. Design and fabrication

The pin-and-socket interconnect consists of a PDMS septum housed in a SU-8 anchor and a non-coring needle that punctures the septum to establish the macro-micro interface. The PDMS septum size and shape is defined by the layout of the SU-8 anchor. Anchor thickness is dictated by the desired flow resistance (determined by the outer diameter (OD) of the needle) and practical limits of fabricating thick film SU-8 structures (including film uniformity and process time). In this work, the SU-8 structure height was selected to be 100–200 μm greater than the OD of the needle. For a 33-gauge needle (OD 203 μm) the SU-8 layer was 300 μm thick, for a 30-gauge needle (OD 305 μm) the SU-8 layer was 500 μm thick.

The SU-8 anchors mechanically interlock with the PDMS septum preventing septum damage or removal during needle insertion and removal. Three anchor shapes (square, circular, and barbed) were fabricated and examined (Fig. 2). The length of the septum also determines the contact length between the needle and PDMS. Thus, there exists a design trade-off between interconnect strength and footprint.

The SU-8 anchor was fabricated on a glass slide substrate. For devices in which electrical traces were required, Parylene C was deposited between the glass substrate and the SU-8 to provide electrical isolation, but was also found to alleviate the thermal stress-induced delamination of the SU-8 [16]. The difference in the coefficient of thermal expansion of the glass slide (8.9×10^{-6}/°C) compared to SU-8 ($5.2 \times 10{-}5$/°C) can result in delamination of SU-8 structures during processing.

Interconnects were fabricated at the inlet and outlet of a single SU-8 microchannel. The interconnect was also integrated into a simple microfluidic system that contained a microchannel, microchambers, electrolysis pump, and resistive sensors without the need for any additional masks (Fig. 3).

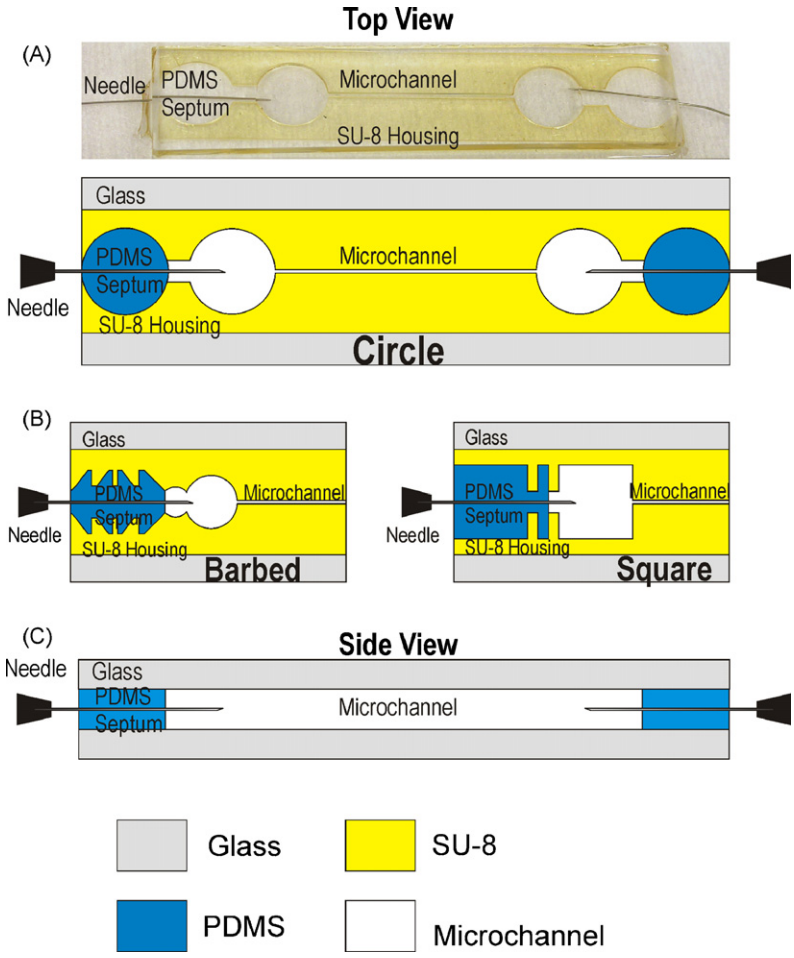

Fig. 2. (A) Image of an assembled circle septum interconnect. (B) Top view of three different septum connector shapes (circle, square, barbed) that were designed and integrated into the test microfluidic system. Needle, PDMS septum, SU-8 housing, and microchannel in the designs are indicated. (C) Side view of the needle piercing the PDMS septum. Image is not drawn to scale.

3.1. System fabrication

Microfluidic systems each containing one channel and integrated interconnects at both the inlet and outlet were batch-fabricated using conventional micromachining techniques (Fig. 4). First, the substrate, either a 76 mm (3 in.) soda lime wafer (Silicon Quest International, Santa Clara, CA) or soda lime slide substrate (75 mm × 50 mm, Corning Glass Works, Corning, NY), was spin coated with AZ 4400 photoresist (AZ Electronic Materials, Branchburg, NJ) (4 krpm, 40 s, 4 μm) (Fig. 4A). After exposure, a liftoff mask was produced. Ti/Pt (200 Å/2000 Å) (International Advanced Materials, Spring Valley, NY) was e-beam evaporated and defined using standard liftoff processes by removing the photoresist layer in acetone, isopropyl alcohol, and deionized water (Fig. 4B). The resistive thermal sensors and electrolysis electrodes were formed with this process. Parylene C (Specialty Coating Systems, Inc., Indianapolis, IN) was vapor deposited (2 μm thick) to electrically isolate the metal traces (Fig. 4C). A 4 μm layer AZ 4400 was spin coated (4 krpm, 40 s), patterned, and used as an etch mask for oxygen plasma removal of Parylene C by reactive ion etching to reveal the contact pads (Fig. 4D).

Next, a 300 μm layer of SU-8 2100 (MicroChem Corp., Newton, MA) was obtained by using a two-step spin coating process to provide better thickness uniformity across the substrate. The first coat was spun at 1.5 krpm (approximately 200 μm thick)

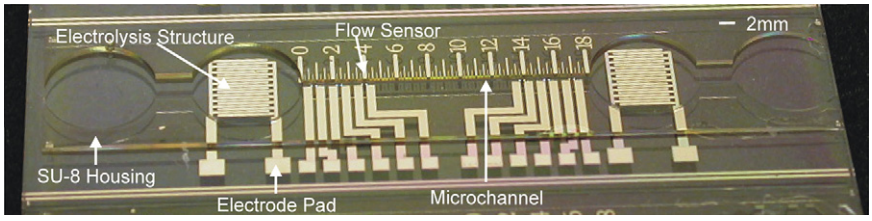

Fig. 3. Integrated interconnect with microfluidic system. System contains SU-8 layer which defines the septum housing, microchambers, and microchannel. Electrolysis structure and flow sensors are fabricated with a Ti/Pt metal layer. PDMS septum and glass cover plate are not present.

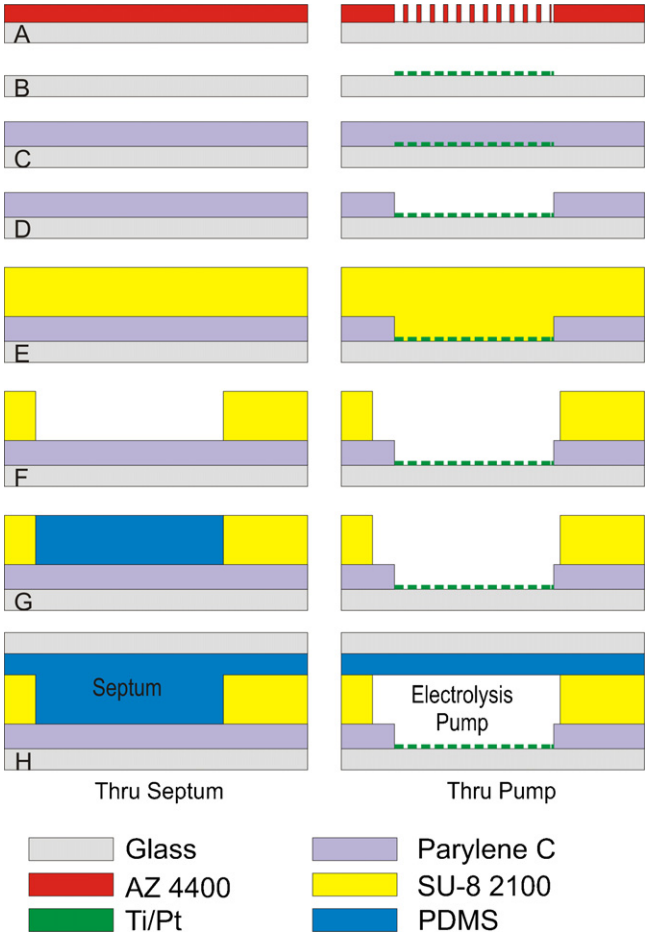

Fig. 4. Simplified fabrication process for the microfluidic chip with integrated interconnect. Cross-section views are through the PDMS septum and microchamber with interdigitated electrodes for an electrolysis pump.

followed by a second planarization coating spun at 3 krpm (for an additional 100 μm) (Fig. 4E). After each spin coat, the applied SU-8 layer rested at room temperature for 3 h to improve planarization. Then, the layers were each softbaked at 90 °C; the first layer softbaked for 90 min and the second for 3 h. Baking steps were all performed on a programmable hotplate (Dataplate Series 730, Barnstead International, Debuque, IA) set to ramp at 3 °C/min. The lower softbake temperature was selected to avoid thermal degradation of the underlying Parylene C. Substrates were allowed to slowly cool to room temperature after each bake step to avoid thermal stress cracks in the SU-8. The SU-8 was patterned (600 mJ/cm^2), post-exposure baked for 30 min at 90 °C, and then developed using SU-8 developer (MicroChem Corp., Newton, MA) (Fig. 4F). A final hardbake step was performed at 90 °C for 30 min.

3.2. Septum formation

The SU-8 layer includes the microchannel which is terminated on either end by a region reserved for the PDMS septum (Sylgard 184, Dow Corning, Midland, MI). A PDMS septum is located at both the input and output and allows rapid access to the sealed microchannel (Figs. 1 and 2). Mechanical interlocking structures patterned in the SU-8 layer secure the PDMS septa

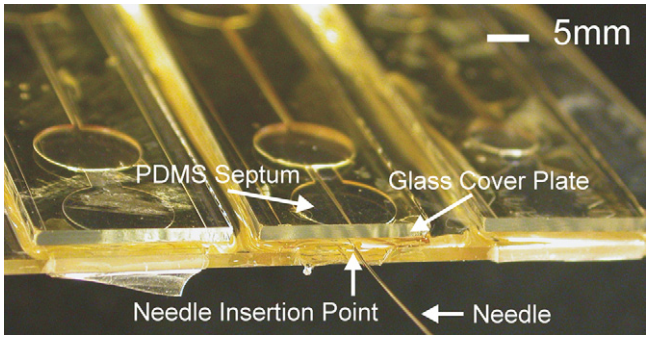

Fig. 5. Edge view of the needle insertion location. The 33-gauge non-coring needle pierces the PDMS septum through the edge of the system, creating an in-plane connection.

to the substrate during both needle insertion and removal. These mechanical anchors were filled with PDMS as follows (Fig. 4G). First, the regions adjacent to the septum (microchambers and microchannel) were filled with deionized water injected with a syringe. Water serves as a convenient mask that prevents PDMS prepolymer from flowing into water-masked areas. PDMS is oil-based and is thus immiscible in water, allowing water to serve as a mold for casting PDMS [17]. PDMS also has a low surface energy and its hydrophobic property further enhances the water masking technique. A similar water masking technique has been previously demonstrated [18,19]. PDMS was mixed in a 10:1 elastomer-to-curing agent ratio (AR-250 Hybrid Mixer, Thinky Corp., Tokyo, Japan) to obtain the prepolymer and then precisely introduced into the septum area through a 20-gauge needle and syringe. PDMS prepolymer was degassed in an evacuated chamber to remove trapped bubbles and then partially-cured (65 °C for 20 min) in order to facilitate the final adhesion of the capping layer.

To complete the microfluidic system, the top of the microchannel was formed by capping the SU-8 channel and PDMS septum with a soda lime glass slide (75 mm × 50 mm × 1 mm, Corning Glass Works, Corning, NY) (Fig. 4H). First, the glass slide was diced to obtain 10 mm × 50 mm pieces to match the die size. To join the substrate and cover, PDMS was used as an adhesive sealant. A thin, partially-cured PDMS membrane (~300–400 μm thick, 65 °C for 20 min) was placed on top of the substrate chip to prevent excess PDMS from entering the microchannel below. Uncured PDMS prepolymer was spread on top of the partially-cured PDMS membrane as an adhesive layer and the glass cover was placed on top of the microchannel assembly. This prepolymer layer further planarizes any remaining thickness non-uniformity in the SU-8 layer. The entire structure was left at room temperature for 24 h to allow the PDMS to cure completely or rapidly cured at 70 °C for 1 h. Finally, a 33-gauge stainless steel non-coring syringe needle (Hamilton Company, Reno, NV) was manually inserted into the interconnect (Fig. 5).

4. Experimental methods

To optimize the performance of this new microfluidic interconnect method, needle tip types were evaluated. The performance of the interconnects was then evaluated using a needle

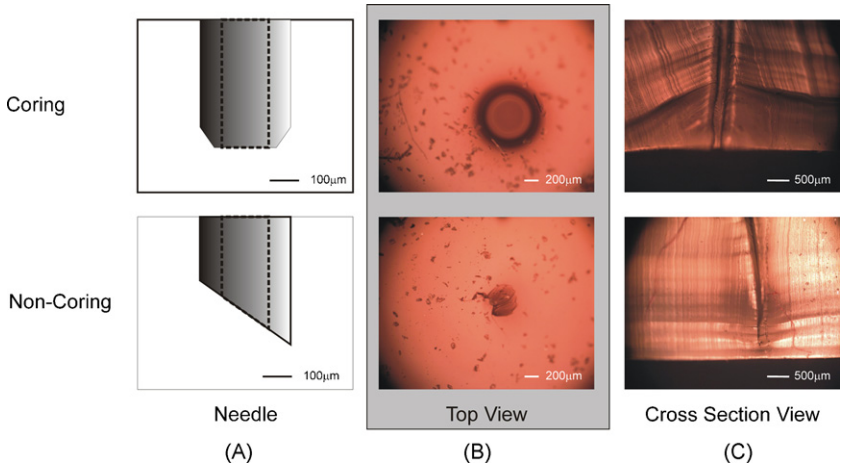

Fig. 6. (A) Comparison of 30-gauge coring and non-coring needle tip shapes. (B) Top and (C) cross-section views of needle tracks through PDMS membranes are shown.

with the most suitable tip type. The robustness and reusability of the needle-septum connection was evaluated by measuring the pull-out forces associated with needle removal. Leakage was examined in both short- and long-term studies under pressurized operation.

4.1. Coring versus non-coring needle tip type

Access to a microchannel was gained by piercing a needle through the PDMS septum such that the lumen of the needle established a continuous fluidic path to the microchannel. Stainless steel coring and non-coring needles (Hamilton Company, Reno, NV) (30-gauge) were examined to determine the needle tip type that could maximize the lifetime of the interconnect [14]. PDMS membranes were casted and cured (1.85 mm thick). A coring or non-coring needle was inserted through each membrane and then removed. The membrane was then dissected through the needle puncture site and optically imaged (Fig. 6).

4.2. Pull-out force and reusability

The reusability of the interconnects was assessed by determining the pull-out forces required to remove the needle after multiple insertions into the same septum. For these experiments, a 33-gauge non-coring needle was used and the three-septum shapes were each evaluated. The microfluidic system was mounted such that the microchannel was oriented perpendicular to the ground by using a custom laser machined test setup (Mini/Helix 800, Epilog, Golden, CO) (Fig. 7). The needle was inserted through a hole in the base of the test fixture and then through the PDMS septum to gain access to the microchannel. Pull-out forces were applied to the needle by gradually increasing the brass weights contained in a bag attached to the needle. The bag was preloaded with a 50 g brass weight. Weights were then added incrementally with a 10 min pause between weight additions to allow the system to equilibrate. The smallest weight used was 1 g which corresponds to a force resolution of 9.8 mN. The total weight attached to the needle was recorded after the needle was pulled out of the septum. The resulting pull-out force was calculated from the final pull-out weight and recorded. The same interconnect was used repeatedly in up to 8 trials following the same procedure described above.

4.3. Maximum operating pressure

The operating range of each of the three interconnect designs was determined for both pressurized dyed water and nitrogen gas. Non-coring needles were inserted through the input and output septums. Dyed water was introduced from the input, through the microchannel, and to the output needle to ensure a continuous fluidic pathway between the input and output. The output needle was blocked (P-656 luer lock assembly and P-770 plug, Upchurch Scientific, Oak Harbor, WA) and the input needle was attached to a custom pressure testing system (Fig. 8).

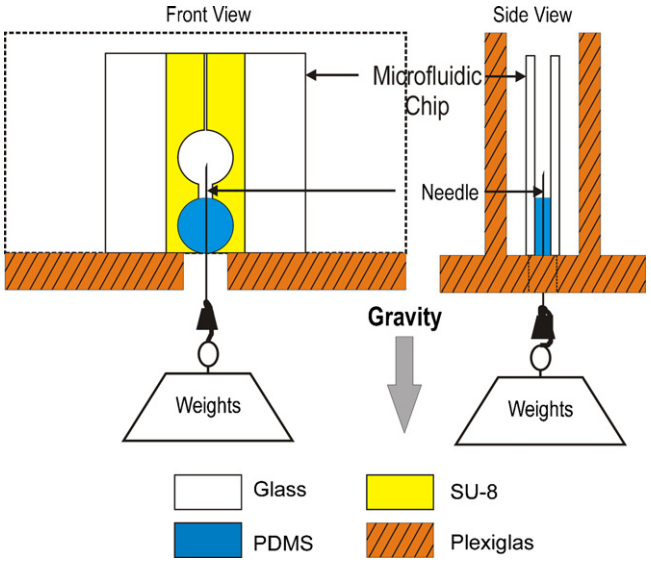

Fig. 7. Pull-out test setup. Connector is held perpendicular to the ground by placing the microfluidic device in the Plexiglas test fixture. Weights are added to a container attached to the luer lock portion of the needle. Pull-out force is determined by multiplying gravity by the combined mass of the weights, needle, and container. Image is not drawn to scale.

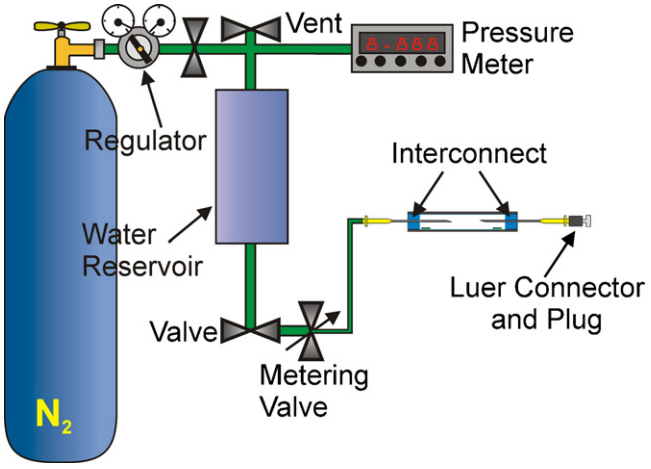

Fig. 8. Test setup for leakage pressure test and prolonged pressure test using pressurized water. Output needle is blocked using an Upchurch plug.

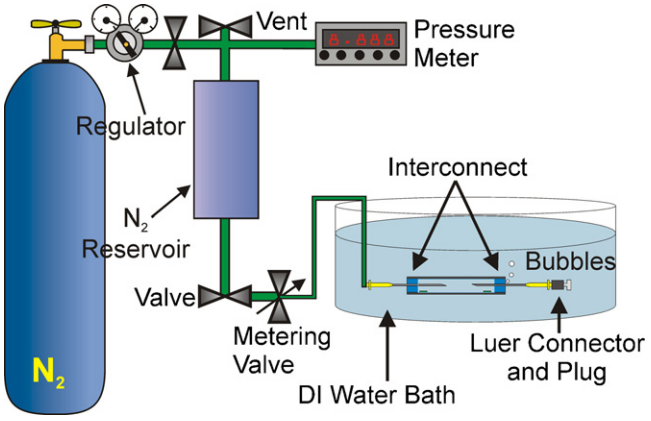

Fig. 9. Test setup for leakage pressure test using pressurized N_2. Leakage is visualized by N_2 bubbles escaping from the submerged the microfluidic chip.

Pressure was slowly increased with a 10 min pause between pressure increments to allow the system to equilibrate. Leakage was determined by directly noting the leakage location when using dyed water. The interconnect assembly was placed on an absorbent cloth to facilitate leakage observation. When using pressurized nitrogen gas, the assembly was submerged in deioinized water and the escape of nitrogen bubbles was used to determine leakage failure (Fig. 9). The pressure at which the interconnect started to leak and the location of the leakage were recorded.

4.4. Prolonged pressure operation

Long-term operation of the interconnects under pressurized water was also evaluated. The same custom pressure testing system was used (Fig. 9). An interconnect was pressurized at 36 kPa and monitored over a 24 h period. This pressure value is half of the average value of the maximum operating pressures for water.

5. Results and discussion

5.1. Coring versus non-coring

30-gauge (OD 305 μm) coring and non-coring needles were compared to determine which needle would facilitate interconnect reusability. The non-coring needle displaced the PDMS material as it moved through the PDMS slab. The displaced material resealed behind the needle as the needle was removed (Fig. 6B–C). The coring needle removed material as it was pushed into the PDMS; a cylindrical pathway was observed when the needle was removed (Fig. 6B–C). The permanent pathway becomes a potential leakage site, which limits interconnect reusability. After inserting the needle, the cylindrical PDMS core remained inside the shank of the needle and effectively clogged the fluid path.

5.2. Pull-out force and reusability

The pull-out forces for each septum shape were obtained and for a single pull-out trial, theoretical maximum (1.19 N) and minimum (0.86 N) pull-out force for interconnects were obtained from (4) using the values in Table 1. The wide range in theoretical values is attributed to the variation published values for the Young's modulus of PDMS [15,20]; differences in material properties may arise due to varying processing conditions (e.g. temperature and time for PDMS curing). The pull-out force for the first removal with respect to contact length and contact area for the circle, square, and barbed interconnect was compared to other pull-out values for published connectors (Fig. 10 and Table 2) [9,13,21]. As predicted in the simple fiber/matrix

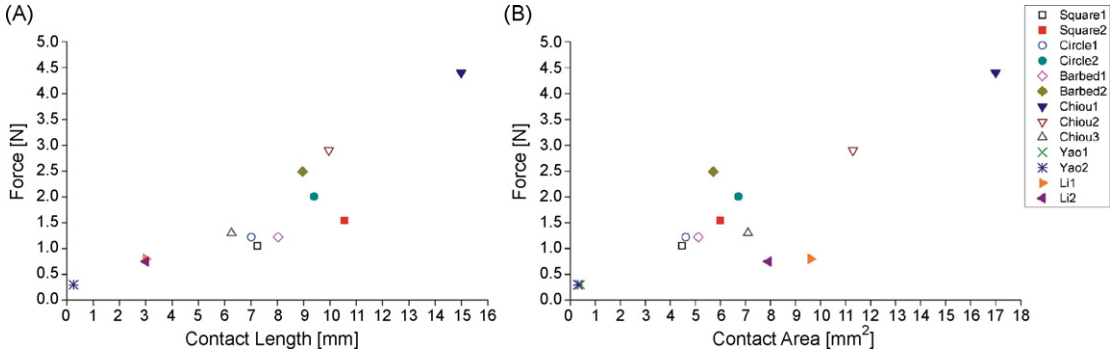

Fig. 10. Comparison of the first pull-out force with respect to (A) contact length and (B) contact area for our interconnects (circle, square, barbed) and that of other published interconnects.

Table 1
Values used to calculate theoretical pull-out force

Variable	Value
E_m	360–870 kPa
G_a	180–240 J/m^2
r	101.5 μm
μp	0.1 kPa
A	2.1 mm^2

model, pull-out force increased with interconnect contact length and contact area. It is important to note that Gent and Liu modeled pull-out of stainless steel fibers from PDMS that were embedded into the material before curing. The model may not adequately account for the increase in compressive force experienced by the needle as it is inserted into the PDMS septum or the irregular path the needle may take. The first pull-out force value for the square, circular, and barbed interconnects may vary from the model due to the inability to precisely determine the contact length and area. The flexible, small diameter needle was manually inserted and the angle and precise location of needle insertion varied between interconnects. It is possible that some interconnects may have been inserted near or at the glass or SU-8 interfaces. Thus, an incomplete PDMS-to-needle seal would result in which the PDMS would compress the needle against the hard surface instead of completely surrounding it. Deviations from the linear behavior predicted by the model may further be attributed to the differences in operating principle between each interconnect system and the fiber/matrix materials used.

The pull-out force data for multiple trials (up to 8 pull-outs) were compared to the performance of other published microfluidic interconnects (Fig. 11A) [9,13,21]. The measured pull-out force was consistent over 8 pull-outs and in some cases, exhibited a slight decrease after the first pull-out. Again, pull-out force was dependent on the contact area between the interconnect fiber and matrix. The pull-out force was normalized with respect to contact area in order to better compare the pull-out force of the existing interconnects (Fig. 11B). Most of the normalized pull-out forces fell within the range of 0.1–0.5 N/mm^2.

Each of the mechanical anchoring schemes for the interconnects (square, circular, barbed) prevented the septum from dislodging from the SU-8 housing. Though all of the interconnect shapes survived multiple uses, the circular shaped anchor may be the most desirable structure for two reasons. First, the circular shape does not contain as many corners that may allow for stress concentration in the SU-8 layer. Secondly, the smooth, circular septa did not contain sharp corners and were easier to fill with PDMS. In the square and barbed septum cavities, the PDMS prepolymer required manual spreading to ensure complete filling of the cavity corners.

Table 3
Results from leakage pressure tests

Port type	Test medium	Leakage pressure (kPa)	Leakage location
Circle	Water	36.27	Between glass and parylene interface
Square	Water	20.82	Between glass and parylene interface
Barbed	Water	51.37	Needle insertion at output
Circle	N_2	60.4	Between glass and parylene interface
Square	N_2	25.72	Needle insertion at output
Barbed	N_2	15.72	Between glass and parylene interface

5.3. Pressurized testing

The leakage test identified the maximum operating pressure as well as the failure mode in each case (Table 3). The maximum operating pressure was 51 kPa for water operation (barbed interconnect) and 60.4 kPa for N_2 operation (circle interconnect). Two failure modes were present: (1) the needle insertion point and (2) at the glass–parylene interface. The first failure mode suggests the presence of a leakage path along the needle insertion path or a compromise of the seal between the needle and the PDMS septum (Fig. 12).

5.4. Prolonged pressure operation

The prolonged pressure test demonstrated that the connector can maintain pressurized water at a pressure of 36.2 kPa for over

Table 2
Comparison of existing interconnects

Connector	Diameter (mm)	Contact length (mm)	Contact area (mm^2)	Fiber material	Matrix material
Circle 1	0.203	7.010	4.471	Stainless Steel	Sylgard 184
Circle 2	0.203	9.400	5.995	Stainless Steel	Sylgard 184
Square 1	0.203	7.240	4.617	Stainless Steel	Sylgard 184
Square 2	0.203	10.540	6.722	Stainless Steel	Sylgard 184
Barbed 1	0.203	8.030	5.121	Stainless Steel	Sylgard 184
Barbed 2	0.203	8.960	5.714	Stainless Steel	Sylgard 184
Chiou 1	0.361	14.990	17.000	Fused Silica	Sylgard 184
Chiou 2	0.361	9.960	11.296	Fused Silica	Sylgard 184
Chiou 3	0.361	6.260	7.100	Fused Silica	Sylgard 184
Yao 1	0.500	0.250	0.393	Glass	MRTV1 American Safety Technologies, Inc.
Yao 2	0.400	0.250	0.314	Glass	MRTV1 American Safety Technologies, Inc.
Li 1	1.020	3.000	9.613	Teflon (PTFE)	Sylgard 184
Li 2	0.840	3.000	7.917	Glass	Sylgard 184

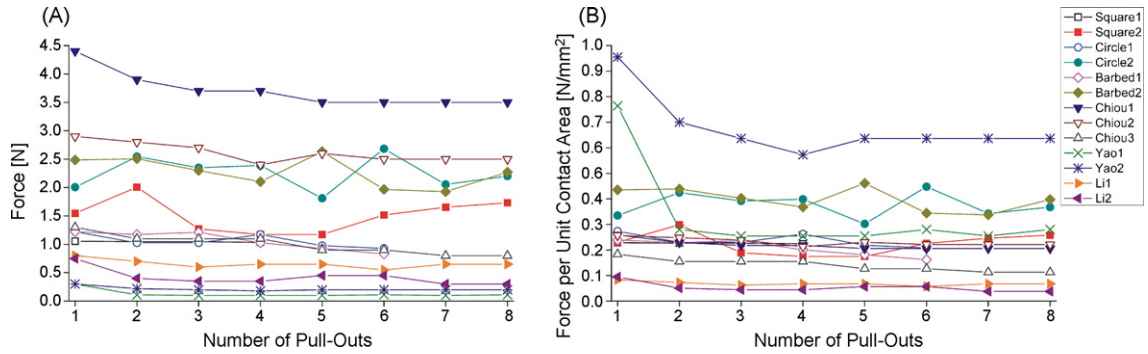

Fig. 11. (A) Comparison of the pull-out force for our interconnects (circle, square, barbed) compared to other published connectors. Pull-out force varies over subsequent pull-outs and is dependent on contact area. (B) Comparison of normalized pull-out force with respect to contact area.

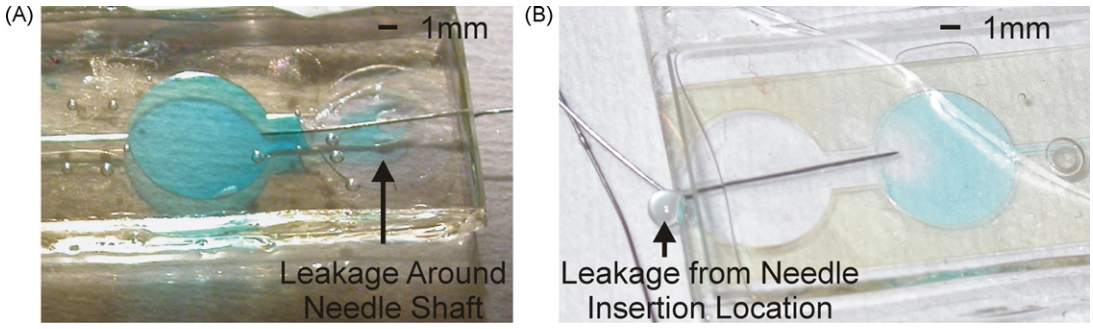

Fig. 12. Interconnect failure at the PDMS septum and stainless steel needle interface. (A) Water surrounds the needle shaft as PDMS is debonded from the needle and (B) seeps from the needle insertion point.

24 h. No measurable leakage was observed over this period of time.

5.5. Failure modes

Needle insertion angle through the input and output septums was observed to be a critical factor in interconnect failure. When the needle was inserted at a downward angle relative to the glass substrate, the tip of the needle would penetrate into the parylene layer and could potentially become lodged at the glass/parylene interface. When a test medium, such as dyed deionized water, was introduced through the needle, the fluid was observed seeping into the interface (Fig. 13). The parylene delaminated from the glass substrate and the interconnect failed. Subsequent fabrication runs were modified to include an adhesion promotion step with silane-based A-174 prior to parylene deposition to prevent parylene delamination from the glass substrate. In these interconnects, if the needle was inserted at an angle, the needle tip would scratch the parylene but the film would not readily delaminate from the glass surface. Conversely, another failure mode occurred when the needle was inserted at an upward angle relative to the glass substrate. The needle could become lodged in the PDMS/glass interface where its circumference was not completely sealed by PDMS. When the needle was inserted immediately adjacent to the glass cap, the needle was not surrounded by PDMS. The small gaps between the needle shaft and the displaced PDMS form low resistance leakage paths (Fig. 12).

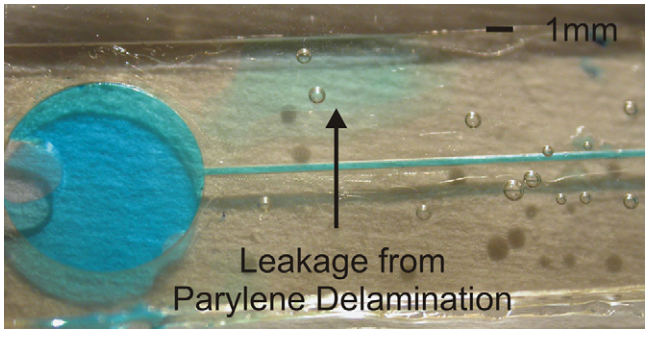

Fig. 13. Interconnect failure due to Parylene C delamination. Dyed water can be seen spreading between the Parylene C and substrate layers.

Misalignment of the needle may occur as the needle penetrates the PDMS septum at an angle parallel to the plane of the substrate. In this case, the needle trajectory would cause the needle tip to collide with the surrounding SU-8 housing and thus block the lumen of the needle. The needle could be removed and reinserted; however, it was demonstrated that repeated insertions were associated with decreasing needle pull-out forces. Thus, careful alignment of the needle to the microchamber is necessary to avoid degradations in interconnect strength related to multiple misaligned needle insertions.

A future refinement to this interconnect would be to include a needle insertion guide, either external or integrated, to prevent failure modes resulting from the needle penetrating through the PDMS septum boundaries and into interfaces. The needle guide would direct the needle to the center of the PDMS septum and prevent the needle from being inserted at an angle. For high density microfluidic connections, multiple interconnects can be

positioned in a linear array at the edges of a microfluidic chip. This interconnect format would be analogous to ribbon cables and sockets on jumper pins commonly found in the microelectronics industry.

6. Conclusion

Practical in-plane integrated interconnects that can be batch-fabricated with microfluidics have been demonstrated. Needle pull-out force was modeled as debonding in which both frictional and adhesion forces were accounted for. In this model, pull-out force scales with needle/septum contact length and this trend was confirmed in experiments and by comparisons with other published interconnects. The reusability of the interconnects was demonstrated in multiple pull-out trials in which the pull-out force remained constant over 8 trials. In experiments which the interconnects were subjected to incrementally increasing gas or water pressure, the Parylene C-to-glass interface adhesion was found to be critical in preventing leakage. Also needle insertion angle and alignment affected the robustness of this interconnect scheme. No leakage was observed under prolonged exposure to pressurized water.

Acknowledgement

This work was funded in part by the Engineering Research Centers Program of the National Science Foundation (NSF) under Award Number EEC-0310723 and an NSF CAREER grant under Award Number EEC-0547544. The authors would like to thank Mr. Merrill Roragen for fabrication assistance, Dr. Tuan Hoang for valuable discussions, and other members of the Biomedical Microsystem Lab at the University of Southern California for their contributions to this work.

References

[1] C.M. Ho, Y.C. Tai, Micro-electro-mechanical-systems (MEMS) and fluid flows, Annu. Rev. Fluid. Mech. 30 (1998) 579–612.
[2] G.M. Whitesides, The origins and the future of microfluidics, Nature 442 (2006) 368–373.
[3] A.V. Pattekar, M.V. Kothare, Novel microfluidic interconnectors for high temperature and pressure applications, J. Micromech. Microeng. 13 (2003) 337–345.
[4] A. Puntambekar, C.H. Ahn, Self-aligning microfluidic interconnects for glass- and plastic-based microfluidic systems, J. Micromech. Microeng. 12 (2002) 35–40.
[5] Z. Yang, R. Maeda, Socket with built-in valves for the interconnection of microfluidic chips to macro constituents, J. Chromatogr. A 1013 (2003) 29–33.
[6] A.M. Christensen, D.A. Chang-Yen, B.K. Gale, Characterization of interconnects used in PDMS microfluidic systems, J. Micromech. Microeng. 15 (2005) 928–934.
[7] P. Galambos, G.L. Benavides, M.O.M.W. Jenkins, D. Hetherington, Precision alignment packaging for microsystems with multiple fluid connections, in: Proceedings of the 2001 ASME Conference, New York, New York, Nov. 11–16, 2001, 2001, pp. 1–8.
[8] E.S. Lee, D. Howard, E. Liang, S.D. Collins, R.L. Smith, Removable tubing interconnects for glass-based micro-fluidic systems made using ECDM, J. Micromech. Microeng. 14 (2004) 535–541.
[9] S.F. Li, S.C. Chen, Polydimethylsiloxane fluidic interconnects for microfluidic systems, IEEE Trans. Adv. Packaging 26 (2003) 242–247.
[10] S. Matsumoto, J. Xie, Y.-C. S Tai, Polymer micro interface for fluidic probing, in: Proceedings of the 10th International Conference on Miniaturized Systems for Chemistry and Life Sciences Squaw Valley, California, 2003, pp. 551–554.
[11] E. Meng, S.Y. Wu, Y.C. Tai, Silicon couplers for microfluidic applications, Fresen. J. Anal. Chem. 371 (2001) 270–275.
[12] S.J. Baldock, P.R. Fielden, N.J. Goddard, H.R. Kretschmer, J.E. Prest, B.J.T. Brown, Novel variable volume injector for performing sample introduction in a miniaturised isotachophoresis device, J. Chromatogr. A 1042 (2004) 181–188.
[13] C.H. Chiou, G.B. Lee, Minimal dead-volume connectors for microfluidics using PDMS casting techniques, J. Micromech. Microeng. 14 (2004) 1484–1490.
[14] R. Lo, K. Kuwahara, P.Y. Li, R. Agrawal, M.S. Humayun, E. Meng, A passive refillable intraocular MEMS drug delivery device, in: IEEE Int. Conf. Microtech. Medicine Biology, IEEE, Okinawa, Japan, 2006, p. 4.
[15] A.N. Gent, G.L. Liu, Pull-out and fragmentation in model fiber composites, J. Mater. Sci. 26 (1991) 2467–2476.
[16] M. Despont, H. Lorenz, N. Fahrni, J. Brugger, P. Renaud, P. Vettiger, High-aspect-ratio, ultrathick, negative-tone near-UV photoresist for MEMS applications, in: Proceedings of the IEEE Micro Electro Mechanical Systems (MEMS'97), Nagoya, Japan, 1997, pp. 518–522.
[17] S.H. Chao, R. Carlson, D.R. Meldrum, Rapid fabrication of microchannels using microscale plasma activated templating (microplat) generated water molds, Lab. Chip 7 (2007) 641–643.
[18] P.-Y. Li, J. Shih, R. Lo, B. Adams, R. Agrawal, S. Saati, M.S. Humayun, Y.-C. Tai, E. Meng, An electrochemical intraocular drug delivery device, in: Proceedings of the IEEE Micro Electro Mechanical Systems (MEMS'07), IEEE, Kobe, Japan, 2007, pp. 15–18.
[19] P.-Y. Li, J. Shih, R. Lo, R. Agrawal, S. Saati, M.S. Humayun, Y.-C. Tai, E. Meng, An electronic intraocular drug delivery device, Sens. Actuators A: Phys. (2008).
[20] D. Armani, C. Liu, N. Aluru, Re-configurable fluid circuits by PDMS elastomer micromachining, in: Proceedings of the IEEE Micro Electro Mechanical Systems (MEMS'99), Orlando, FL, 1999, pp. 222–227.
[21] T.-J. Yao, S. Lee, W. Fang, Y.-C. Tai, Micromachined rubber o-ring microfluidic couplers, in: Proceedings of the IEEE Micro Electro Mechanical Systems (MEMS'00), Institute of Electrical and Electronics Engineers Inc, Piscataway, NJ, USA, Miyazaki, Japan, 2000, pp. 624–627.

Biographies

Ronalee Lo received her BS degree in engineering from Harvey Mudd College in 2001. She worked at a Washington, D.C. based Biotechnology consulting firm, BioStar, for one year prior to enrolling at the University of Southern California to pursue a PhD. She received a MS in Biomedical Engineering Medical Devices and Diagnostics from the University of Southern California in 2004. Ronalee is currently a member of the Biomedical Microsystems Laboratory where her current research focuses are on MEMS drug delivery devices and microfluidic interconnects.

Ellis Meng received her BS degree in engineering and applied science from the California Institute of Technology in 1997. She pursued her graduate studies in electrical engineering and received her MS in 1998 and PhD in 2003 at the same institution. She is now an assistant professor of Biomedical Engineering at the University of Southern California. In the National Science Foundation Biomimetic MicroElectronic Systems Engineering Research Center (BMES ERC) she is a Thrust Leader for Interface Technology and the Associate Director of Education and Student Diversity. She is a member of Tau Beta Pi, the Institute of Electrical and Electronics Engineers (IEEE), the American Society of Mechanical Engineers (ASME), the Society of Women Engineers (SWE), and the Biomedical Engineering Society (BMES). Dr. Meng is a recipient of the NSF CAREER award and was recently appointed the Viterbi Early Career Chair in the Viterbi School of Engineering.